






## ARTICLE OPEN ACCESS

# Infrared Thermography in Plant Factories: Solving Spatiotemporal Variations Via Machine Learning

Avinash Agarwal<sup>1,2</sup>  | Filipe de Jesus Colwell<sup>3</sup> | Rosalind Dinnis<sup>1</sup> | Viviana Andrea Correa Galvis<sup>3</sup>  | Tom R. Hill<sup>4</sup>  | Neil Boonham<sup>1</sup>  | Ankush Prashar<sup>1</sup> 

<sup>1</sup>School of Natural and Environmental Sciences, Newcastle University, Newcastle upon Tyne, UK | <sup>2</sup>Institute for Bio- and Geosciences: Plant Sciences (IBG-2), Forschungszentrum Jülich GmbH, Jülich, Germany | <sup>3</sup>Crop Science R&D Division, Infarm - Indoor Urban Farming B.V., Amsterdam, the Netherlands | <sup>4</sup>Faculty of Medical Sciences, Newcastle University, Newcastle upon Tyne, UK

**Correspondence:** Ankush Prashar ([ankush.prashar@newcastle.ac.uk](mailto:ankush.prashar@newcastle.ac.uk)) | Avinash Agarwal ([avinash.agarwal.1612@gmail.com](mailto:avinash.agarwal.1612@gmail.com), [a.agarwal@fz-juelich.de](mailto:a.agarwal@fz-juelich.de))

**Received:** 18 March 2024 | **Revised:** 25 February 2025 | **Accepted:** 27 February 2025

**Funding:** This work was funded by Innovate UK (Technology Strategy Board—CR&D) [grant number: TS/V002880/1].

## ABSTRACT

Infrared thermography (IRT) for real-time stress detection in plant factories (PFs) remains largely unexplored. Hence, this study investigates the feasibility of implementing IRT in PFs, using machine learning (ML) to address the challenges in information processing. Herein, purple basil plantlets were subjected to root dehydration within a pilot-scale PF, and canopy temperature was monitored at regular intervals using a thermal camera. Subsequently, eight ML models using the ‘support vector machines’ algorithm were tested for stress detection. Our findings revealed that differences in canopy temperature due to microenvironmental variations led to inaccurate representation of stress. Nonetheless, binary classification models trained using plants at medial and high stress overcame this issue by identifying stressed samples with 81%–94% accuracy. However, although models trained with medially stressed samples performed well for all stress levels, models trained using highly stressed samples failed to identify medial stress reliably. Additionally, ternary and quaternary classification models were able to identify unstressed samples but could not distinguish between different levels of stress. Hence, binary classification models trained using medially stressed samples overcame spatiotemporal variations in canopy thermal profile most effectively and provided probabilistic estimates of plant stress within the PF most consistently.

## 1 | Introduction

Plant water status is a crucial factor influencing crop growth and yield as it plays an important role in physiological signalling as well as the biosynthesis and transport of nutrients, carbohydrates, and various other metabolites [1–3]. Additionally, plant water status also acts as an indicator of stress by influencing temperature regulation via stomatal opening [4–6]. Any biotic or abiotic stress that disrupts water uptake results in the closure of stomata due to loss of turgor pressure, which in turn impedes transpirational cooling of leaves, increasing canopy temperature [7]. This increment in canopy temperature occurs

before plant water status is affected markedly, making it a useful trait for early stress detection.

Considering the sensitivity of plant temperature to physiological perturbations, infrared thermography (IRT) has gained popularity in recent years for real-time monitoring of plant stress [7–9]. Since IRT accurately senses fluctuations in canopy temperature, its pertinence in high-throughput real-time crop stress monitoring has been assessed with special emphasis on water stress and crop performance [10–12]. Further, the scope of using IRT has been well-explored for crop production systems such as fields, greenhouses, and growth chambers [5, 8, 13–17].

This is an open access article under the terms of the [Creative Commons Attribution](https://creativecommons.org/licenses/by/4.0/) License, which permits use, distribution and reproduction in any medium, provided the original work is properly cited.

© 2025 The Author(s). *Modern Agriculture* published by Wiley-VCH GmbH.

## Summary

- Crop stress detection in plant factories via thermal imaging may be challenging because perceptible plant temperature is strongly influenced by its microenvironment.
- Thermal image analysis via supervised machine learning allows the development of robust prediction models for identifying stressed plants by overcoming these limitations.
- Binary classification models can be used for reliably identifying stressed plants and estimating the level of plant stress in plant factories.

However, the potential of utilising this technology remains largely unexplored for plant factories (PFs), that is, modern indoor vertical farms which utilise tiered or stacked hydroponic plant growth units along with LED lighting and artificial air circulation for high density crop cultivation.

Despite better regulation of the growth environment within PFs [18], plants are still vulnerable to stress due to biotic or abiotic stressors [19]. Furthermore, high-density planting increases the likelihood of rapid widespread crop loss if the stress is not mitigated timely. Since plant growth in PFs is extensively automated, with minimal human intervention, introduction of fast high-throughput plant monitoring systems that complement any alerts coming from hardware failures is necessary for ensuring quality production. Thus, IRT may be deemed as an ideal tool for real-time crop monitoring in PFs owing to its rapid response, sensitivity, ease of use, and high throughput.

Due to the high dimensionality of thermal images, analysing IRT data may prove to be challenging via conventional mathematical tools. However, the process may be streamlined by implementing machine learning (ML). In recent years, ML has emerged as a useful tool for high-throughput analysis of image-based datasets as it enables rapid in-depth processing of numerical and spatial data patterns [20–23]. Amongst the various ML approaches, supervised learning via support vector machines (SVMs) has been frequently employed for detecting plant stress using multispectral, thermal, and hyperspectral imaging [24–27] as it creates hypothetical boundaries in high-dimensional space for optimal separation between different dataset classes [28]. Hence, integrating SVM-based ML classification with IRT could significantly improve real-time crop monitoring within PFs.

In the present study, we explored the feasibility of IRT for real-time stress detection in PFs using purple basil (*Ocimum basilicum* L. var. *purpurascens*) as a model system. Since implementation of IRT for plant stress detection in PFs has not been investigated extensively till date, we carried out an exploratory study to reveal potential bottlenecks in this process. For this, we imposed stress on the plants by withholding irrigation to elicit changes in canopy temperature, and monitored the plants at regular intervals via thermal imaging to obtain spatiotemporal trends. The information was used to develop a framework by combining IRT with ML for real-time plant stress detection.

## 2 | Methods

### 2.1 | Plant Material

Purple basil seedlings were raised in coco-peat plugs (Van der Knapp, The Netherlands) in a nursery chamber (Aralab-InFarm UK Ltd., London, UK); each plug received 10 seeds for germination. At ~2 cm, the seedlings were transferred to a small-scale PF (InStore Farm, InFarm UK Ltd.; Figure 1A) located at the Agriculture Building, Newcastle University, UK. Briefly, the PF consisted of an enclosed growth chamber with eight hydroponic trays (80 × 80 cm<sup>2</sup>), each having an 8 × 8 array of empty slots (Figure 1B). Each tray received 58 seedling plugs, and the six remaining slots were used for temperature references, irrigation, and handling (Figure 1B). Broad-spectrum LED arrays having an approximate red (400–499 nm):green (500–599 nm):blue (600–699 nm) distribution of 40:20:40 were used to maintain the light intensity at 280 μmol/m<sup>2</sup>sec PPFD, following a 16/8 h day-night cycle (Figure 2). A commercial hydroponic fertiliser mix was used as the nutrient source, and irrigation was performed following the nutrient film technique using an electrical pump. Temperature and relative humidity (RH) were maintained at 25 ± 1°C and 60 ± 5%, respectively, through a centralised air circulation vent connected to a custom-made heating, ventilation, and air-conditioning (HVAC) system that delivered air at 0.3 m/s at the canopy level [29]. Growth conditions and irrigation were regulated automatically through a Farmboard (InFarm UK Ltd.) via built-in sensors for temperature and RH as well as nutrient solution flow rate, electrical conductivity, and pH. Additionally, commercial handheld temperature and RH sensors (EasyLog EL-USB-2-LCD, Lascar Electronics, UK) were used to monitor the growth environment close to each tray to ensure uniform conditions throughout the setup.

### 2.2 | Experimental Design

Plants were subjected to water stress after 2 weeks of growth. Two preliminary trials (PTs) were carried out to get a general overview of stress responses induced by water deficit, followed by a third (main) trial aimed at ML-based stress detection (Figure 2). In the first trial (PT-1), irrigation was stopped at 8 a. m., and thermal imaging (described later) was carried out with five separate trays for 0, 6, 12, 22, and 34 h without irrigation. Twelve samples were randomly selected from the corresponding tray immediately after imaging. The aerial part comprising of at least four to five healthy seedlings with fully expanded leaves was considered as the shoot, whereas the remaining portion comprising the coco-peat plug embedded with the root hairs was considered as the ‘root-plug’ (Supporting Information Figure S1A). Fresh weight (FW) of the shoots and root-plugs was measured immediately, followed by oven drying at 85°C for 48 h to measure the dry weight (DW). Subsequently, each root-plug was soaked in tap water for an hour, and the weight of water-saturated plugs was also recorded. Shoot water content and relative water content of root-plugs were calculated as follows:

$$\text{Shoot water content (\%)} = 100 \times \frac{(\text{Shoot FW} - \text{Shoot DW})}{\text{Shoot FW}} \quad (1)$$

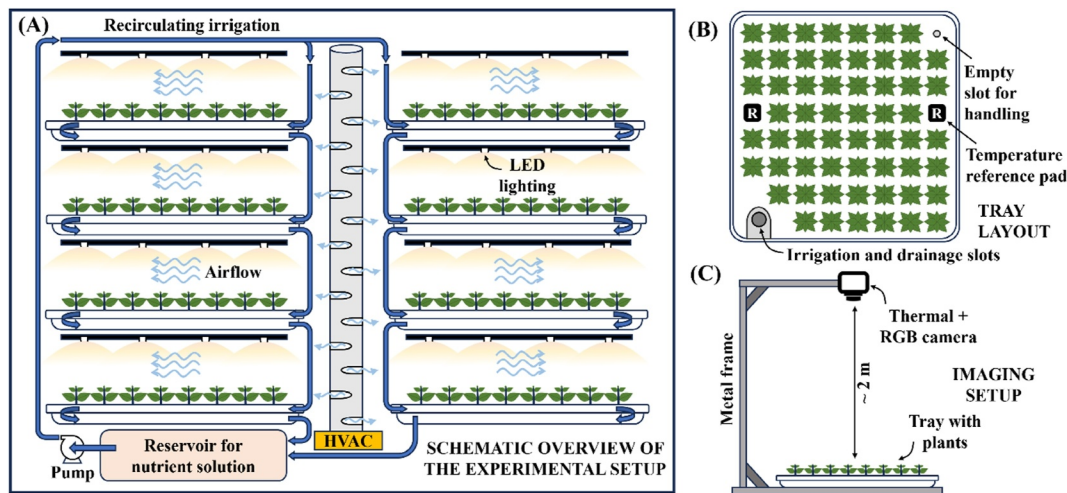


**FIGURE 1** | Schematic overview of the experimental plant factory (A), layout of the planting tray (B), and the setup for imaging (C). HVAC, customised heating, ventilation, and air-conditioning unit connected to the air circulation vent. LED spectrum: red (400–499 nm); green (500–599 nm); blue (600–699 nm) distribution of 40:20:40; light intensity: 280  $\mu\text{mol}/\text{m}^2\text{sec}$  PPFD; day/night cycle: 16/8 h; air temperature:  $25 \pm 1^\circ\text{C}$ ; relative humidity:  $60 \pm 5\%$ ; rate of air flow: 0.3 m/s.

|               | Time                | 5 am | 6 am | 7 am | 8 am | 9 am | 10 am | 11 am | 12 pm | 1 pm | 2 pm | 3 pm | 4 pm | 5 pm | 6 pm | 7 pm | 8 pm | 9 pm | 10 pm | 11 pm |     | 5 am | 6 am | 7 am |     | 5 pm | 6 pm | 7 pm | Hrs without irrigation at imaging |
|---------------|---------------------|------|------|------|------|------|-------|-------|-------|------|------|------|------|------|------|------|------|------|-------|-------|-----|------|------|------|-----|------|------|------|-----------------------------------|
| <b>Trials</b> | Lights <sup>^</sup> | ■    | ■    | ■    | ■    | ■    | ■     | ■     | ■     | ■    | ■    | ■    | ■    | ■    | ■    | ■    | ■    | ■    | ■     | ■     | ... | ■    | ■    | ■    | ... | ■    | ■    | ■    |                                   |
| PT-1*         | Tray 1              |      |      |      |      |      |       |       |       |      | •    |      |      |      |      |      | ○    |      |       |       | ... |      |      |      |     |      |      |      | 0                                 |
|               | Tray 2              |      |      |      |      |      |       |       |       |      | •    |      |      |      |      |      |      |      |       |       | ... |      |      |      |     |      | ○    |      | 6                                 |
|               | Tray 3              |      |      |      |      |      |       |       |       |      |      |      |      |      |      |      | •    |      |       |       | ... |      |      |      |     |      | •    |      | 12                                |
|               | Tray 4              |      |      |      |      |      |       |       |       |      |      |      |      |      |      |      |      |      |       |       | ... |      |      |      |     |      | •    |      | 22                                |
|               | Tray 5              |      |      |      |      |      |       |       |       |      |      |      |      |      |      |      |      |      |       |       | ... |      |      |      |     |      | •    |      | 34                                |
| PT-2**        | Tray 1              |      |      |      |      |      |       |       |       | •    |      |      |      |      | •    |      |      |      |       |       | ... |      |      |      |     |      |      |      | 5, 10                             |
|               | Tray 2              |      |      |      |      |      |       |       |       |      | •    |      |      | •    |      |      |      |      |       |       | ... |      |      |      |     |      |      |      | 7, 9                              |
|               | Tray 3              |      |      |      |      |      |       |       |       |      | •    |      |      |      |      |      | •    |      |       |       | ... |      |      |      |     |      |      |      | 6, 12                             |
|               | Tray 4              |      |      |      |      |      |       |       |       |      |      |      | •    |      |      | •    |      |      |       |       | ... |      |      |      |     |      |      |      | 8, 11                             |
|               | Control             |      |      |      |      |      |       |       |       | ○    |      |      | ○    |      |      | ○    |      |      |       |       | ... |      |      |      |     |      |      |      | 0                                 |
| MT            | Tray 1              |      |      |      |      |      |       |       |       |      | •    | •    | •    | •    | •    | •    | •    |      |       |       | ... |      |      |      |     |      |      |      | 6–12                              |
|               | Tray 2              |      |      |      |      |      |       |       |       |      | •    | •    | •    | •    | •    | •    | •    |      |       |       | ... |      |      |      |     |      |      |      | 6–12                              |
|               | Control             |      |      |      |      |      |       |       |       |      | •    | •    | •    | •    | •    | •    | •    |      |       |       | ... |      |      |      |     |      |      |      | 0                                 |
|               | Control             |      |      |      |      |      |       |       |       |      | •    | •    | •    | •    | •    | •    | •    |      |       |       | ... |      |      |      |     |      |      |      | 0                                 |

**Legends:**

- Lights ON
- Lights OFF
- Irrigation ON
- Irrigation OFF
- Thermal image acquisition at the start of the hour, irrigation turned/remains ON after imaging
- Thermal image acquisition at the start of the hour, irrigation remains OFF after imaging
- Thermal image acquisition for confirming stability in temperature, data not shown

**FIGURE 2** | Overview of the experimental design indicating the lighting and irrigation schedules along with intervals for thermal imaging. \*After imaging, 12 random samples were taken for fresh and dry biomass measurements. \*\*After imaging, five random samples were used for measuring stomatal conductance and biomass. <sup>^</sup>Lighting schedule was the same for all trials.

$$\text{Root plug (RP) relative water content (\%)} = 100 \times \frac{(\text{RP FW} - \text{RP DW})}{(\text{FW of saturated RP} - \text{RP DW})} \quad (2)$$

The next trial (PT-2) was performed to track the onset of stress by comparing plant temperature with stomatal conductance and root-plug water content at earlier stages of water

deprivation. As before, irrigation was stopped at 8 a.m., and thermal imaging was performed using four trays at eight hourly intervals from 5 to 12 h without irrigation, wherein each tray was used for two random intervals (Figure 2). Immediately after imaging, five plants were selected from the respective tray for recording stomatal conductance using an AP4 Porometer (Delta-T Devices, Cambridge, UK; range: 0.025–3 cm/s; accuracy: > 90% for 0.025–3 cm/s), along with

the relative water content of root-plugs being calculated as before.

Findings of PT-1 and PT-2 were used to design the main trial. In this trial, thermal imaging of unirrigated plants was performed for two horizontally adjacent trays at hourly intervals from 6 to 12 h without irrigation (Figure 2). This data was used for assessing spatiotemporal variations in perceived plant temperature, followed by ML for stress detection. All trials were performed with at least one tray as a control to monitor the temperature in continuously irrigated plants. A gap of 2 hours was maintained between turning the lights ON (6 a.m.) and stopping of irrigation (8 a.m.) for allowing the plants to ‘wake up’ completely, that is, get acclimated to the light.

### 2.3 | Thermal Imaging

Thermal imaging was performed using a T1030sc thermal camera (Teledyne FLIR LLC, USA; temperature range:  $-40^{\circ}\text{C}$ – $150^{\circ}\text{C}$ ; accuracy:  $\pm 1\%$  for  $5^{\circ}\text{C}$ – $150^{\circ}\text{C}$ ), having  $7.5\text{--}14\ \mu\text{m}$  spectral range and focal plane array uncooled microbolometer with HD detector (resolution:  $1024 \times 768$  pixels). The camera acquired thermal and RGB images simultaneously. Plant canopies were imaged outside the growth chamber using a customised setup for maintaining a fixed vertical distance ( $\sim 2\text{ m}$ )

between the camera and the tray surface (Figure 1C), adjacent to the growth chamber to ensure similar environmental conditions. Imaging was performed under a neutral-white LED light source at a room temperature of  $25 \pm 1^{\circ}\text{C}$ . Camera parameters such as reflected, atmospheric, and optics temperatures were fixed, and customised black body temperature reference pads were placed on each tray for the entire duration of the experiment [30]. Each tray was imaged within 30 s of being taken out of the growth chamber and returned immediately.

### 2.4 | Thermal Image Pre-Processing and Temperature Extraction

Pre-processing of thermal images was performed using Python programming ([www.python.org](https://www.python.org)) implementing the *flirextractor* library (<https://pypi.org/project/flirextractor>). The pipeline for this involved the following steps (Figure 3): (1) parallax correction between the thermal and RGB images for background (tray) removal using RGB colour thresholding; (2) temperature mapping ( $15^{\circ}\text{C}$ – $30^{\circ}\text{C}$  scale) to grayscale (0–1 scale); (3) isolation of individual plants using an  $8 \times 8$  grid to get 64 regions of interest (size:  $95 \times 95$  pixels); (4) removal of unusable images; and (5) temperature extraction, followed by normalisation as an environmental correction for absolute errors. Average plant temperature was computed after excluding a

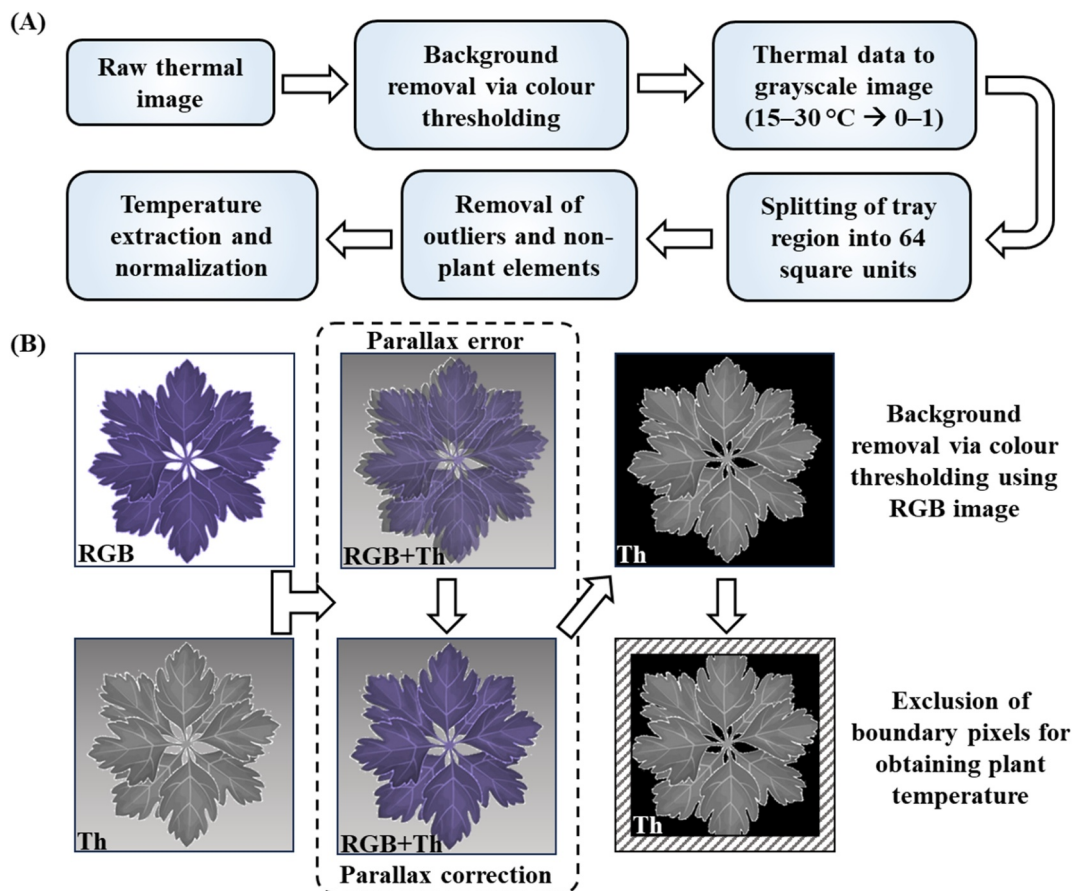


**FIGURE 3** | Overview of the image pre-processing pipeline (A) and a flowchart depicting parallax correction, background removal, and selection of region of interest for extracting plant temperature (B). RGB, colour image having Red, Green, and Blue channels; Th, thermal image; RGB + Th, overlaid RGB and thermal images for representing parallax error and its correction.



region of 10 pixels on all four sides of each plant to minimise the effect of overlapping leaves from adjacent samples (Figure 3B). Only the leaves visible at the canopy level were considered while estimating sample temperature; no other parts of the plant (stem, roots) were considered in this process.

The difference between observed plant temperature and reference temperature ( $T_{ref}$ ), that is, the mean temperature of the black body reference pads, was used along with a constant ( $25^{\circ}\text{C}$ ) to obtain normalised sample temperature as follows:

$$\text{Normalised temperature } (^{\circ}\text{C}) = \text{Observed temperature} + (25 - T_{ref}) \quad (3)$$

Positional effects on perceived plant temperature within different regions of each tray were visualised by combining the data for both trays to get the average sample temperature at different positions within the trays (Supporting Information Figure S2).

## 2.5 | ML for Predicting Plant Stress

Thermal images from the main trial were used to design a Python-based ML pipeline implementing SVMs for identifying stressed plants (Supporting Information Figure S3). For this, we used the *svm* function of the Scikit-learn library [31]. Prior to training the models, eight-fold data augmentation was performed by rotating and inverting each image (Supporting Information Figure S4). Considering the radial canopy distribution of each sample, this data augmentation process helped overcome any potential biases arising from the spatial distribution of image pixels that were not perceptible visually, and created larger and more diverse training datasets, which is beneficial for reducing overfitting of ML models [32]. Other types of data augmentation steps, such as blurring and zooming in/out, were not used for the sake of simplicity keeping in mind the practical possibilities of such monitoring systems during commercial use.

Subsequently, each thermal image was flattened to a vector containing the values for each pixel within the image. A randomized stratified train-test split of 80:20 was implemented. All models were allowed to choose from three kernels, viz., *linear*, *polynomial*, and *radial basis function (rbf)*, along with a broad range of hyperparameters  $C$  (0.01–10) and  $\gamma$  (0.001–1) with the

target of maximising accuracy (Supporting Information Table S1). Here,  $C$  is the cost parameter defining the penalty weight of deviations, and  $\gamma$  is an *rbf*-specific parameter controlling the trade-off between bias errors and variance in the adjusted model. The same hyperparameter sets were used for five-fold cross-validation to check model performance for variations in training datasets.

In order to simplify the depiction of ML analyses, samples from each imaging interval have been represented using incremental stress levels (SL) as SL0, SL1, SL2, SL3, SL4, SL5, and SL6 for 6, 7, 8, 9, 10, 11, and 12 h without irrigation, respectively. Based on the results of PT-1 and PT-2, samples from 6 h without irrigation, that is, the SL0 class, were considered as ‘unstressed’. Six ML models were generated for binary classification (BC), along with one model each for ternary and quaternary classification (TC, QC). Each BC (two-class) model was trained using SL0 images along with images from one of the six other classes (SL1–SL6) as the stressed sample set, and the models were labelled as BC-1 to BC-6, respectively. Similarly, the TC (three-class) and QC (four-class) models were generated using images from SL0, SL3, and SL6 (representing no, medium, and high stress, respectively) and images from SL0, SL2, SL4, and SL6 (representing no, mild, moderate, and high stress, respectively). The number of images used from each class for training and testing has been summarised in Table 1.

Model performance was assessed using the test dataset (20%) to calculate accuracy, *Precision*, *Recall* (sensitivity), *F1 score*, and *Specificity* (Table 2) using the confusion matrix. Here, each of the five performance parameters represents a unique aspect of model ‘confusion’, that is, the ability or inability to distinguish different classes robustly. In particular, ‘accuracy’ provides a general overview of model performance, whereas the other four parameters provide class-specific insights into model behaviour. The predictive ability of all ML models was further tested by individually deploying each model to analyse all samples from SL0–SL6 (Supporting Information Table S2), followed by plotting sample temperature against its Platt’s probabilistic estimate of stress provided by the respective ML model.

## 2.6 | Statistical Analysis

Data pertaining to shoot and root-plug water content as well as plant temperature were subjected to one-way ANOVA followed

**TABLE 1** | Summary of machine learning dataset from the main trial.

| Class | Imaging interval (h) | No. of images |           |                |            |
|-------|----------------------|---------------|-----------|----------------|------------|
|       |                      | Original      | Augmented | Training (80%) | Test (20%) |
| SL0   | 6                    | 113           | 904       | 723            | 181        |
| SL1   | 7                    | 111           | 888       | 710            | 178        |
| SL2   | 8                    | 112           | 896       | 717            | 179        |
| SL3   | 9                    | 112           | 896       | 717            | 179        |
| SL4   | 10                   | 112           | 896       | 717            | 179        |
| SL5   | 11                   | 107           | 856       | 685            | 171        |
| SL6   | 12                   | 109           | 872       | 697            | 175        |

Abbreviation: SL, stress level.

**TABLE 2** | Model performance parameters calculated from the confusion matrix.

| Parameter    | Formula  | Remarks   |
|--------------|--|---|
| Accuracy (%) | $100 \times \text{total no. of TP for all groups} \div \text{total no. of samples}$      | Indicates the overall performance of the model considering all classes  |
| Precision    | $\text{TP} \div (\text{TP} + \text{FP})$   | Share of correct classifications within each predicted class            |
| Recall       | $\text{TP} \div (\text{TP} + \text{FN})$   | Proportion of correctly classified samples from each original class     |
| F1 score     | $2 \times \text{Precision} \times \text{Recall} \div (\text{Precision} + \text{Recall})$ | Parameter indicating classification ability of the model for each class |
| Specificity  | $\text{TN} \div (\text{TN} + \text{FP})$   | Goodness of model at identifying negative outcomes for each class       |

Abbreviations: FN, False negative; FP, False positive; TN, True negative; TP, True positive.

by Tukey's post hoc test ( $p < 0.05$ ) in Python using the *scipy.stats* library (<https://docs.scipy.org/doc/scipy/reference/stats.html>) to ascertain the significance of differences.

### 3 | Results

#### 3.1 | Plant Stress Response

Data from the first preliminary trial (PT-1) revealed a gradual decline in shoot and root-plug water content, along with a steady increase in plant temperature from 0 to 34 h without irrigation (Supporting Information Figure S5). Notably, while a significant reduction in root-plug water content and an increasing trend in plant temperature was observed from 6 to 12 h (Supporting Information Figure S5A,C), shoot water content did not change significantly ( $p < 0.05$ ) over the same interval (Supporting Information Figure S5B). PT-2 data for 5–12 h without irrigation indicated that root-plug water content decreased at a rate of  $\sim 15\%/h$  between 5 and 7 h without irrigation (Figure 4A). However, it remained relatively stable between 7 and 10 h, followed by the continuation of water loss at a slower pace of  $\sim 6\%/h$  between 10 and 12 h (Figure 4A). Additionally, reduction in root-plug water content below *ca.* 30%–35% and stomatal conductance below *ca.* 0.25–0.3 cm/s was accompanied by a rapid increase in plant temperature (Figure 4B,C).

In the main trial, a significant increase of *ca.* 2°C ( $p < 0.05$ ) in average plant temperature was noted from 6 to 12 h without irrigation (Figure 4D). A positional effect was evident within the tray area (Figure 5), wherein samples closer to the air circulation vent consistently appeared cooler than those at the far edge, despite having similar stress levels in terms of duration without irrigation. Further, higher temperatures were only recorded close to the centre of the tray during later stages.

#### 3.2 | ML Model Performance

Classification reports (Tables 3 and 4) generated from the confusion matrix of each model (Supporting Information Tables S3 and S4) indicate an increase in accuracy and *Precision* by *ca.* 1.7 times from BC-1 to BC-6. In contrast, *Recall*, *F1 score*, and *Specificity* for SL0 (unstressed class) increased by *ca.* 1.25–

1.5 times from BC-1 to BC-6, although the same parameters showed an increment of *ca.* 2.3–2.9 times for the stressed classes. The accuracy of the TC model was only higher than BC-1 and BC-2, whereas the QC model had the lowest overall accuracy (Tables 3 and 4). Five-fold cross-validation using the best-performing modelling parameters (Supporting Information Table S5) yielded similar accuracy values as the respective models (Supporting Information Table S6), indicating consistency in model performance with variations in training and test datasets.

Notably, BC-1 had similar *Precision* for both SL0 (0.53) and SL1 (0.55), although the *Recall* was 0.74 and 0.32 for the two classes, respectively (Table 3). This indicates that while more than half of the samples were classified correctly by this model, most of those samples were SL0. The *F1 score* generalised this inference by combining the outcomes of the previous two parameters. In consensus, the low *Specificity* for SL1 (Table 3) revealed that the BC-1 model was unable to reliably identify samples that did not belong to SL1. Results for BC-2 were comparable, but slightly better (Table 3). In contrast, BC-3 showed the earliest possibility of reliable stress prediction by correctly identifying a majority of the samples from the stressed (SL3) class (115/179; Supporting Information Table S3), with the performance improving steadily until BC-6. Interestingly, *Precision*, *Recall*, *F1 score*, and *Specificity* of the TC model were higher for the two extreme classes, that is, SL0 and SL6, as compared to the intermediate class, viz., SL3. A similar trend was observed for the QC model where the magnitude of these four performance parameters was higher for SL0 and SL6 (extreme classes) as compared to SL2 and SL4 (intermediate classes).

#### 3.3 | Probabilistic Prediction of Plant Stress Via ML Models

Plants with higher temperatures had a greater probability of being detected as 'stressed' using most ML models (Figures 6 and 7). Notably, BC-3 to BC-6 models were able to distinguish between stressed and unstressed plants more robustly than BC-1 and BC-2. A gradual transition in the distribution of the temperature-probability point cloud was observed across the models, from being localised in the 0.4–0.65 probability region for BC-1 (Figure 6A) to two discrete clusters in the 0 and 1 regions for samples with temperatures  $< 22^\circ\text{C}$  and  $> 23^\circ\text{C}$ ,

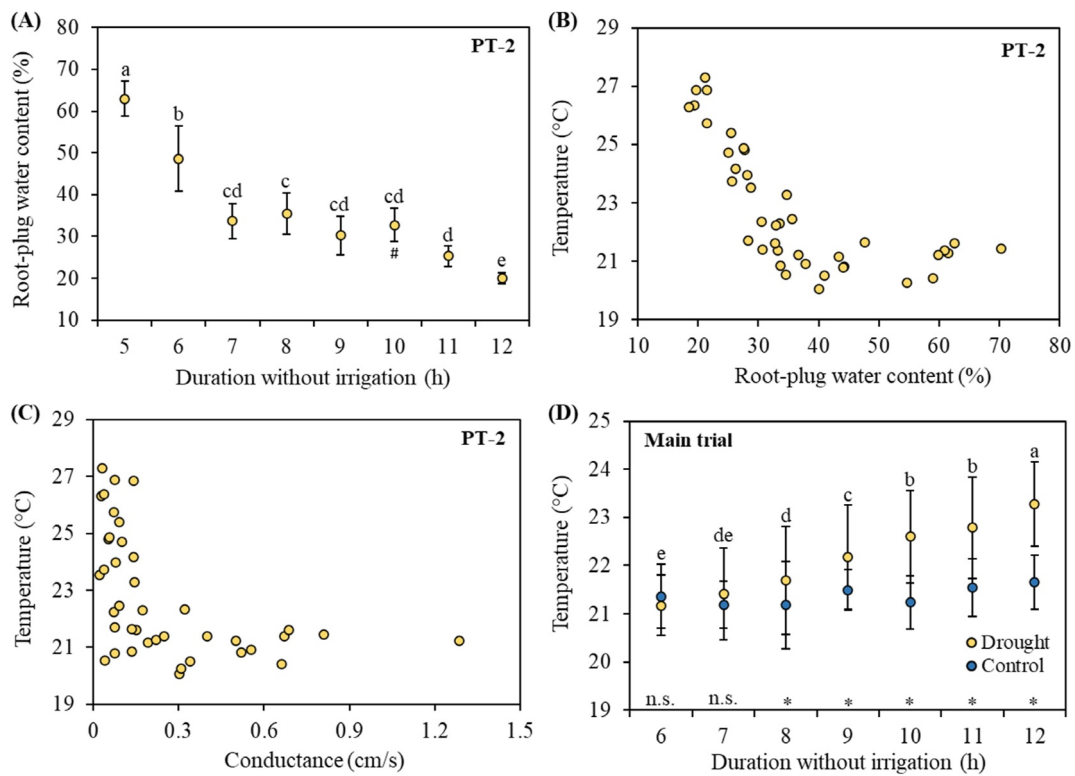


**FIGURE 4** | Root-plug water content at different intervals without irrigation (A;  $n = 5$  for each interval) and the relation of plant temperature with root-plug water content (B;  $n = 39$ ) and stomatal conductance (C;  $n = 39$ ) recorded in the second preliminary trial (PT-2), as well as plant temperature from 6 to 12 h with and without irrigation in the main trial (D;  $n = 116$  for each interval). Values with error bars indicate mean  $\pm$  standard deviation (A, D). Different lower-case letters (a–e) indicate significant differences in means as per Tukey's test ( $p < 0.05$ ) between different intervals without irrigation (A, D). Differences in mean plant temperature between the irrigated (Control) and unirrigated (Drought) plants at each interval have been indicated as significant (\*) or not significant (n.s.) following Tukey's test ( $p < 0.05$ ; D). #One sample had to be omitted from PT-2 at 10 h due to handling error.

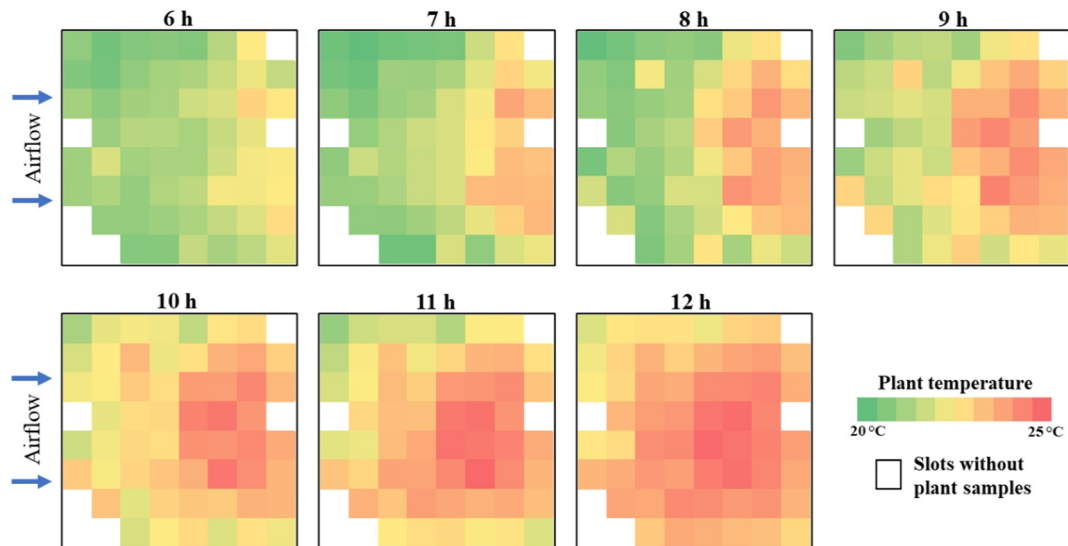


**FIGURE 5** | Heatmaps depicting the spatial variation in temperature within the hydroponic trays from 6 to 12 h without irrigation. Each image represents the average normalised temperature of two replicated trays from the main trial. Slots without plant samples indicate positions on the tray that were used for irrigation, temperature reference pads, or handling, as indicated in Figure 1B.

respectively, for the BC-6 model (Figure 6F). In concurrence with the BC models, the relatively cooler samples had a higher probability of being classified as SL0 or 'unstressed' by the TC

and QC models as well (Figure 7A,D). However, probabilistic predictions for higher levels of stress showed unclear trends for both the TC and QC models (Figure 7B,C,E,F).

**TABLE 3** | Classification report on test data for binary classification (BC) models.

| Model | Class |     | Accuracy (%) | Precision |      | Recall |      | F1 score |      | Specificity |      | Support |     |
|-------|-------|-----|--------------|-----------|------|--------|------|----------|------|-------------|------|---------|-----|
|       | UC    | SC  |              | UC        | SC   | UC     | SC   | UC       | SC   | UC          | SC   | UC      | SC  |
| BC-1  | SL0   | SL1 | 53.20        | 0.53      | 0.55 | 0.74   | 0.32 | 0.61     | 0.40 | 0.74        | 0.33 | 181     | 178 |
| BC-2  | SL0   | SL2 | 63.05        | 0.59      | 0.77 | 0.90   | 0.36 | 0.71     | 0.49 | 0.89        | 0.37 | 181     | 179 |
| BC-3  | SL0   | SL3 | 73.33        | 0.70      | 0.78 | 0.82   | 0.64 | 0.76     | 0.71 | 0.82        | 0.65 | 181     | 179 |
| BC-4  | SL0   | SL4 | 81.94        | 0.84      | 0.80 | 0.80   | 0.84 | 0.82     | 0.82 | 0.79        | 0.84 | 181     | 179 |
| BC-5  | SL0   | SL5 | 88.92        | 0.88      | 0.90 | 0.91   | 0.87 | 0.89     | 0.88 | 0.90        | 0.88 | 181     | 171 |
| BC-6  | SL0   | SL6 | 93.54        | 0.94      | 0.93 | 0.93   | 0.94 | 0.94     | 0.93 | 0.93        | 0.94 | 181     | 175 |

Abbreviations: SC, Stressed class; SL, stress level; Support, number of samples used from each class during model testing; UC, Unstressed class.

**TABLE 4** | Classification report on test data for ternary and quaternary classification (TC, QC) models.

| Model            | Class            | Precision | Recall | F1 score | Specificity | Support |
|------------------|------------------|-----------|--------|----------|-------------|---------|
| TC               | SL0              | 0.68      | 0.85   | 0.75     | 0.92        | 181     |
|                  | SL3              | 0.54      | 0.32   | 0.40     | 0.66        | 179     |
|                  | SL6              | 0.72      | 0.83   | 0.77     | 0.92        | 175     |
|                  | Accuracy: 66.54% |           |        |          |             |         |
| QC               | SL0              | 0.49      | 0.82   | 0.62     | 0.94        | 181     |
|                  | SL2              | 0.16      | 0.02   | 0.03     | 0.67        | 179     |
|                  | SL4              | 0.39      | 0.41   | 0.40     | 0.80        | 179     |
|                  | SL6              | 0.63      | 0.75   | 0.69     | 0.92        | 175     |
| Accuracy: 49.86% |                  |           |        |          |             |         |

Abbreviations: QC, quaternary classification; SL, stress level; Support, number of samples used from each class during model testing; TC, ternary classification.

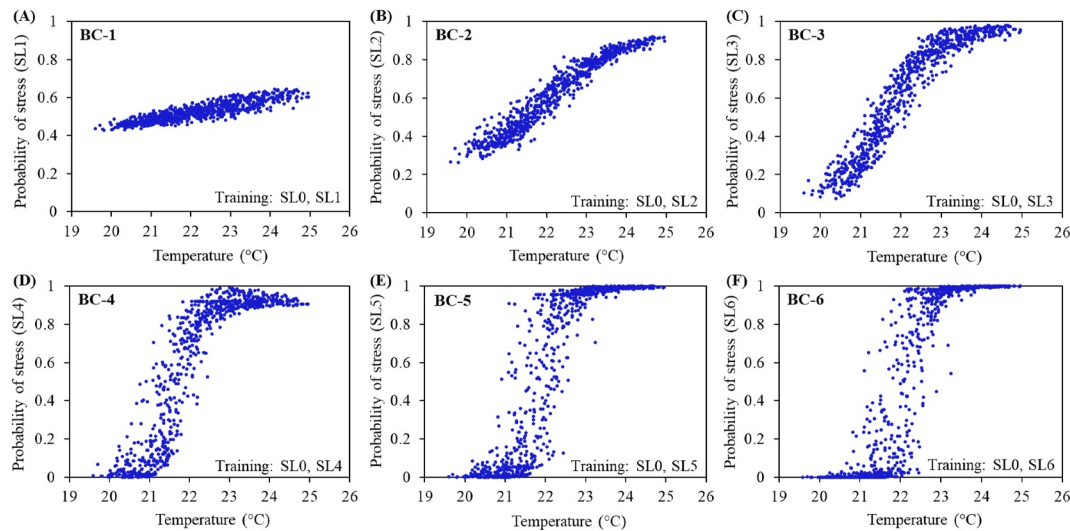


**FIGURE 6** | Plant temperature versus Platt's probability of being classified as stressed by the six binary classification (BC) models. Individual plots present the outcomes for BC-1 to BC-6 models (A–F). Each plot represents the probabilistic prediction for all experimental samples ( $n = 776$ ). Stress level (SL) classes employed for training the respective ML models have been specified within each plot along with the name of the model.

## 4 | Discussion

### 4.1 | Influence of Water Deficit and Plant Position on Canopy Temperature

Decline in shoot turgor pressure due to water deficit in the root region results in stomatal closure, causing a rise in canopy temperature [7, 33, 34]. However, shoot water content and plant

temperature remained relatively unchanged ( $p < 0.05$ ) from 0 to 6 h without irrigation in PT-1, despite significant reduction in relative water content of the root-plugs from 95.5% to 49.8% (Supporting Information Figure S5). This suggests that the moisture content of root-plugs was not low enough to trigger a temperature increase due to stomatal closure until 6 h. However, subsequent reduction in plug water content from 49.8% to 22.8% over the 6–12 h interval (Supporting Information



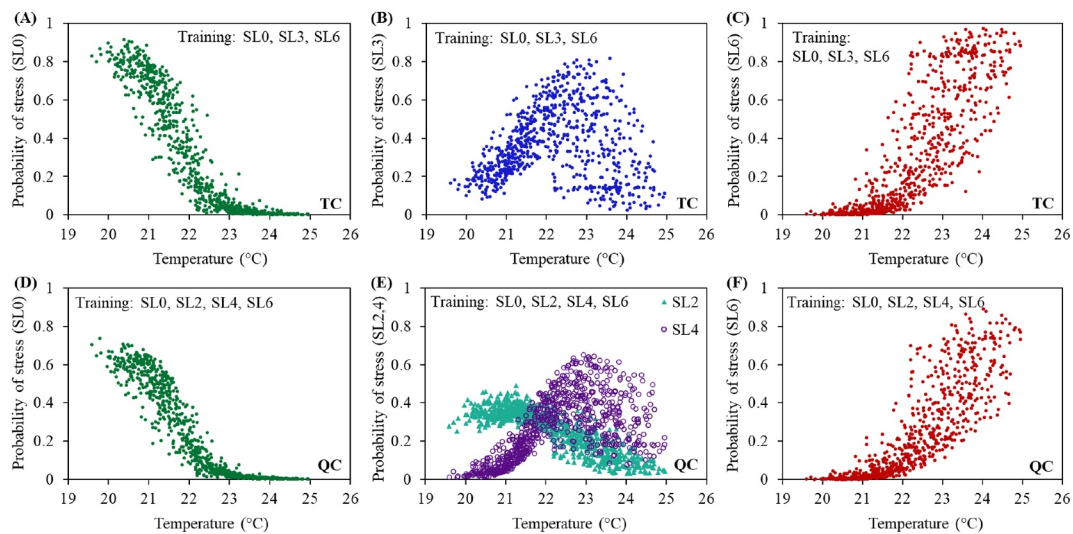


**FIGURE 7** | Plant temperature versus Platt's probability of being classified into different levels of stress by the ternary (TC; A–C) and quaternary (QC; D–F) classification models. Each plot represents the probabilistic prediction for the samples from all intervals ( $n = 776$ ). Stress level (SL) classes employed for training the respective ML models have been specified within each plot along with the name of the model.

Figure S5A) was accompanied by a decline in mean shoot water content by ~12% (Supporting Information Figure S5B) and a concomitant increase in average plant temperature by *ca.* 2°C (Supporting Information Figure S5C). This steady increase in plant temperature marks the triggering of stomatal closure, resulting in reduced transpirational cooling [5, 7], indicating a gradual increment in water deficit stress.

In earlier studies, a significant increase in canopy temperature was reported for plants grown at *ca.* 50% field capacity compared to well-irrigated plants [15, 35]. In contrast, the stability in canopy temperature observed in this study from 0 to 6 h without irrigation in PT-1 may be attributed to the stable RH and adequate moisture in the root-plug, possibly resulting in a relatively stable vapour pressure deficit (VPD) in the growth environment, which delayed stomatal closure [36]. It is worth mentioning here that while VPD is a convenient and reliable measure of plant water status, we have avoided indicating the same owing to its dependence on leaf temperature. Instead, we have used shoot and root-plug water content as more direct measures of plant water status in PT-1 (Supporting Information Figure S5), followed by root-plug water content, stomatal conductance, and plant temperature for PT-2 (Figure 4A–C). Accordingly, co-assessment of these parameters in PT-2 revealed that reduction in plug water content below a certain threshold, that is, *ca.* Thirty-five percent, triggered rapid stomatal closure and consequently caused a steady increase in plant temperature.

Contrary to our expectation of a gradual increment in plant temperature with declining stomatal conductance and root-plug water content in PT-2, we noticed that average canopy temperature remained largely unchanged despite steady reduction in root-plug water content and stomatal conductance until 7 h without irrigation, corresponding to *ca.* 30%–35% and *ca.* 0.25–0.3 cm/s, respectively (Figure 4A–C). However, the temperature increased sharply from 7 h onwards, although root plug water content was relatively stable between 7 and 10 h without irrigation. This shift in plant status was possibly due to widespread

stomatal closure between 6 and 7 h without irrigation and a water deficit response to prevent excessive transpiration and preserve moisture, which also resulted in reduced water uptake from the root-plug. Stability in plant temperature at earlier stages could be expected as a result of air conditioning and forced air circulation. However, the sudden but strong onset of drought response in terms of temperature rise occurred due to rapid stomatal closure, because of which stomatal conductance became too low to maintain transpirational cooling. The situation was likely intensified due to the roots being exposed to air (Supporting Information Figure S1), unlike conventional cultivation systems where the roots are blanketed by soil which would allow changes in root microenvironment at a slower pace. Further studies with diverse plants would help us better understand such behaviours, as roots of hydroponically-grown plants may behave very differently from normal roots.

Nonetheless, plant temperature was found to vary considerably across the tray at each interval (Figure 5) due to positional effects. Specifically, plants located closer to the air circulation vents and the edges were relatively cooler, possibly due to better air circulation and convective heat dissipation. Such observations mark the bottleneck in identifying stressed plants within PFs solely based on absolute temperature thresholds, necessitating a more in-depth analysis of thermal images by ML to identify cohort-based probabilistic trends.

## 4.2 | Comparing ML Performance Parameters for Stress Detection

In general, ML models trained using closer SLs had lower accuracy than the models whose training datasets were further apart. This was especially evident for BC-1, BC-2, TC, and QC as also indicated by the low performance parameter values ( $< 0.5$ ; Tables 3 and 4). This observation could be attributed to similarities in canopy temperature between classes with closer levels

of stress. In addition, positional effects within the tray (Figure 5) increased temperature variance for each SL, making the samples from adjacent SLs even less discernible. However, as the level of stress between the training classes became more distinct, the performance improved steadily.

Moreover, comparison of BC-3 with the TC model, which could be technically considered as an extension of the BC-3 model with an extra SL6 'high stress' class, indicated that having too many classes confused the model. Specifically, despite an overall accuracy of 66.54%, all four class-specific performance parameters for TC (Table 4) indicated that the model was confused while identifying SL3 samples, which were more reliably identified by BC-3 (Table 3). Similarly, the low overall accuracy of the QC model (< 50%) could also be attributed to too many classes, with similarity between samples of adjacent classes increasing model confusion further. Thus, the observations highlight the limitations of SVM-based thermal image classification models trained with too many classes or when samples across the different classes displayed a high degree of similarity.

### 4.3 | Comparing Probabilistic Estimates of Stress by Different ML Models

While the plots for BC-1 and BC-2 (Figure 6A,B) showed limited probabilistic diversity for the likelihood of stress with respect to plant temperature, the BC-3 model yielded a uniform and continuous distribution of points throughout the entire probabilistic range (Figure 6C). Furthermore, although the model was trained with only SL0 (unstressed) and SL3 (medium stress) samples, it was even able to accurately predict a higher probability of stress (> 0.8) beyond ca. 23°C, that is, for samples mostly belonging to SL5 and SL6 (moderate and high stress). While the BC-4 model (Figure 6D) also showed some similarities with BC-3 (Figure 6C), it exhibited an erratic trend at intermediate temperatures (~21.5°C–22.5°C), which became more prominent in BC-5 and BC-6 (Figure 6E,F). This suggests that the latter three models could confidently classify samples with very high or very low levels of stress, whereas 'unknown' samples from intermediate stress levels, that is, SL2 and SL3, might have confused them.

Results for the TC model indicated that while it could distinguish SL0 samples reliably (Figure 7A), it failed to distinguish between SL3 and SL6 as effectively, resulting in an irregular distribution of probabilistic estimates (Figure 7B,C). This was in line with the performance parameters (Table 4), and happened likely due to the higher variability and overlap in canopy temperature between later stages of stress (Figure 4D). The observations were similar for the QC model, with probabilistic classification values for SL0 and SL2 being < 0.7 and < 0.5, respectively (Figure 7D,E), and probability distribution for SL4 and SL6 being highly inconsistent (Figure 7E,F). Thus, the results for TC and QC indicate that models could not identify samples confidently when trained with too many classes having high degrees of similarity.

Since the BC-3 model showed a steady probabilistic transition over the entire temperature range and was even able to reliably

assess the likelihood of stress in samples beyond its training range (Figure 6C), such a model could be deemed most useful for predicting the probability of stress over a continuous scale, especially in real-world scenarios where plant stress needs to be assessed with precision. In contrast, models such as BC-5 and BC-6 could be utilised for a more stringent classification as 'stressed' or 'unstressed', which would work best for detecting high levels of stress.

### 4.4 | Future Perspectives for IRT in Plant Factories

Earlier studies have explored the implementation of ML and IRT for assessing drought stress in field conditions [10, 25] as well as in greenhouses [12]. Our study follows the same principle to assess the potential of IRT for identifying stressed plants within PFs by focussing on spatiotemporal variations, comparison of BC, TC, and QC models, as well as probabilistic prediction of stress. Herein, processing of thermal images via SVM-based classification models takes the spatial distribution of data points for each sample into consideration, which adds an additional layer of information in comparison to using only canopy temperature values. Although many studies are implementing more advanced deep learning algorithms such as neural networks for plant image analysis and stress detection [20, 23], we have utilised SVM for our exploratory investigation to avoid model overfitting, considering the limited sample size. However, tests using more diverse datasets with larger sample sizes must be performed to explore algorithms such as convolutional neural networks and long short-term memory networks for developing more elaborate models. More in-depth SVM hyperparameter tuning could be tried as well.

Our findings also highlight variations in the microenvironment within PFs, and how it influences plant responses that impact sensor readings. Since parameters such as tray size and shape, as well as location and distribution of ventilation openings affect plant microenvironment significantly, designing PFs keeping in mind potential plant monitoring technologies such as IRT is crucial for ensuring compatibility. For instance, uniform distribution of air vents and the use of mixing fans could improve microenvironment consistency in such systems, simplifying thermal image analysis. Moreover, trials comparing prediction accuracies of IRT-based ML models trained with variable and stringently-controlled environmental conditions would provide additional insights for developing a more robust thermal image processing pipeline for commercial-scale PFs using controlled experimental trial data. Additionally, since research related to improving resource-use efficiency in PFs, especially light- and water-use efficiency, is being pursued actively, IRT-based crop monitoring could be helpful in aiding researchers and growers to monitor plant status more accurately while testing new growth protocols.

In general, the technique described in this study can be effectively translated for detecting any abiotic stress where plant temperature is affected, and where visual symptoms are not prominent at early stages, such as stress due to inadequate root aeration, as well as biotic stresses where stomatal response is

affected, such as root infections. Further trials would be helpful in establishing potential applications for such conditions using species-specific models. Additionally, co-assessment of data from other sensors such as multispectral and 3D cameras could be tested in tandem with IRT to further improve crop monitoring within PFs.

## 5 | Conclusion

Rapid growth in the use of PFs over the past decade has revealed various challenges, as well as scopes for improving cultivation in PFs. Since such systems rely extensively upon technology with numerous mechanical components running continuously, any undetected incident resulting in plant stress may have a cascading effect causing extensive crop loss. Hence, early detection of plant stress plays a pivotal role in ensuring productivity in such highly controlled and machine-dependent systems, prompting the adoption of IRT for such operations. The present study highlights the importance of PF system design for incorporating IRT-based crop monitoring via ML, with special emphasis on positional effects within the cultivation area. In addition, our findings indicate that while longer durations of stress made it easier to identify stressed plants, even mild symptoms appearing early could be detected via IRT using ML models. We also found that the use of BC models was adequate for detecting stressed plants reliably, whereas using more than two classes confused the algorithm, especially when differences between the training datasets were not very prominent. Our findings also depict the pitfalls of using absolute temperature for plant stress detection in PFs, emphasising the importance of spatial thermal mapping and ML-based assessment in such systems. Further investigations using other crops and diverse ML approaches with different stresses will broaden the knowledge base for feasibly implementing this technology in commercial PFs.

### Author Contributions

**Avinash Agarwal:** conceptualisation (equal), data curation (equal), formal analysis (lead), investigation (equal), methodology (equal), writing – original draft (lead), writing – review and editing (equal). **Filipe de Jesus Colwell:** conceptualisation (equal), data curation (equal), formal analysis (supporting), investigation (supporting), methodology (equal), validation (equal), writing – review and editing (equal). **Rosalind Dinnis:** data curation (equal), formal analysis (supporting), investigation (supporting), and methodology (supporting). **Viviana Andrea Correa Galvis:** conceptualisation (equal), funding acquisition (equal), project administration (equal), resources (equal), writing – review and editing (equal). **Tom R. Hill:** funding acquisition (equal), project administration (supporting), resources (equal), supervision (supporting), writing – review and editing (equal). **Neil Boonham:** conceptualisation (equal), funding acquisition (equal), investigation (supporting), project administration (lead), resources (equal), supervision (supporting), writing – review and editing (equal). **Ankush Prashar:** conceptualisation (equal), funding acquisition (equal), investigation (equal), resources (equal), supervision (lead), writing – original draft (supporting), writing – review and editing (equal).

### Acknowledgements

We thank the Infarm UK team for supplying seedlings and providing technical support, along with the Infarm Crop Science team (Germany)

for their support. We acknowledge all the partners (RoboScientific, Marks and Spencer, and Infarm) for their feedback and support in the project. We also thank the staff at Newcastle University for their technical, administrative and logistic support. AA thanks Dr. Monica Barman, Leibniz Institute for Vegetable and Ornamental Crops (IGZ) for her guidance on statistical analysis. AA thanks Forschungszentrum Jülich for financial and infrastructural support during manuscript revision.

### Conflicts of Interest

The authors declare no conflicts of interest.

### Data Availability Statement

Data are available from the corresponding authors upon reasonable request.

### References

1. H. Lambers and R. S. Oliveira, “Plant Water Relations,” in *Plant Physiological Ecology* (Springer, 2019), 187–263, [https://doi.org/10.1007/978-3-030-29639-1\\_5](https://doi.org/10.1007/978-3-030-29639-1_5).
2. R. M. Deans, T. J. Brodribb, F. A. Busch, and G. D. Farquhar, “Optimization Can Provide the Fundamental Link Between Leaf Photosynthesis, Gas Exchange and Water Relations,” *Nature Plants* 6, no. 9 (2020): 1116–1125, <https://doi.org/10.1038/s41477-020-00760-6>.
3. M. Ozturk, B. Turkyilmaz Unal, P. Garcia-Caparrós, A. Khursheed, A. Gul, and M. Hasanuzzaman, “Osmoregulation and its Actions During the Drought Stress in Plants,” *Physiologia Plantarum* 172, no. 2 (2021): 1321–1335, <https://doi.org/10.1111/ppl.13297>.
4. M. Gräf, M. Immitzer, P. Hietz, and R. Stangl, “Water-Stressed Plants Do Not Cool: Leaf Surface Temperature of Living Wall Plants Under Drought Stress,” *Sustainability* 13, no. 7 (2021): 3910, <https://doi.org/10.3390/su13073910>.
5. M. Pineda, M. Barón, and M. L. Pérez-Bueno, “Thermal Imaging for Plant Stress Detection and Phenotyping,” *Remote Sensing* 13 (2021): 68, <https://doi.org/10.3390/rs13010068>.
6. K. Brewer, A. Clulow, M. Sibanda, et al., “Estimation of Maize Foliar Temperature and Stomatal Conductance as Indicators of Water Stress Based on Optical and Thermal Imagery Acquired Using an Unmanned Aerial Vehicle (UAV) Platform,” *Drones* 6, no. 7 (2022): 169, <https://doi.org/10.3390/drones6070169>.
7. M. Smigaj, A. Agarwal, H. Bartholomeus, et al., “Thermal Infrared Remote Sensing of Stress Responses in Forest Environments: A Review of Developments, Challenges, and Opportunities,” *Current Forestry Reports* 10, no. 1 (2024): 56–76, <https://doi.org/10.1007/s40725-023-00207-z>.
8. A. Prashar and H. G. Jones, “Infra-Red Thermography as a High-Throughput Tool for Field Phenotyping,” *Agron* 4, no. 3 (2014): 397–417, <https://doi.org/10.3390/agronomy4030397>.
9. P. Waiphara, C. Bourgenot, L. J. Compton, and A. Prashar, “Optical Imaging Resources for Crop Phenotyping and Stress Detection,” in *Environmental Responses in Plants. Methods in Molecular Biology*, eds. P. Duque and D. Szakonyi, Vol. 2494 (Humana Press, 2022), 255–265, [https://doi.org/10.1007/978-1-0716-2297-1\\_18](https://doi.org/10.1007/978-1-0716-2297-1_18).
10. K. Banerjee, P. Krishnan, and N. Mridha, “Application of Thermal Imaging of Wheat Crop Canopy to Estimate Leaf Area Index under Different Moisture Stress Conditions,” *Biosystems Engineering* 166 (2018): 13–27, <https://doi.org/10.1016/j.biosystemseng.2017.10.012>.
11. S. Das, J. Chistopher, A. Apan, et al., “Evaluation of Water Status of Wheat Genotypes to Aid Prediction of Yield on Sodic Soils Using UAV-Thermal Imaging and Machine Learning,” *Agricultural and Forest Meteorology* 307 (2021): 108477, <https://doi.org/10.1016/j.agrformet.2021.108477>.



12. P. M. P. Correia, J. Cairo Westergaard, A. Bernardes da Silva, T. Roitsch, E. Carmo-Silva, and J. Marques da Silva, "High-Throughput Phenotyping of Physiological Traits for Wheat Resilience to High Temperature and Drought Stress," *Journal of Experimental Botany* 73, no. 15 (2022): 5235–5251, <https://doi.org/10.1093/jxb/erac160>.
13. A. Prashar, J. Yildiz, J. W. McNicol, G. J. Bryan, and H. G. Jones, "Infra-Red Thermography for High Throughput Field Phenotyping in *Solanum tuberosum*," *PLoS One* 8, no. 6 (2013): e65816, <https://doi.org/10.1371/journal.pone.0065816>.
14. R. S. N. Lima, I. García-Tejero, T. S. Lopes, et al., "Linking Thermal Imaging to Physiological Indicators in *Carica papaya* L. Under Different Watering Regimes," *Agricultural Water Management* 164 (2016): 148–157, <https://doi.org/10.1016/j.agwat.2015.07.017>.
15. S. Biju, S. Fuentes, and D. Gupta, "The Use of Infrared Thermal Imaging as a Non-Destructive Screening Tool for Identifying Drought-Tolerant Lentil Genotypes," *Plant Physiology and Biochemistry* 127 (2018): 11–24, <https://doi.org/10.1016/j.plaphy.2018.03.005>.
16. A. Khorsandi, A. Hemmat, S. A. Mireei, R. Amirfattahi, and P. Ehsanzadeh, "Plant Temperature-Based Indices Using Infrared Thermography for Detecting Water Status in Sesame under Greenhouse Conditions," *Agricultural Water Management* 204 (2018): 222–233, <https://doi.org/10.1016/j.agwat.2018.04.012>.
17. P. Pipatsitee, A. Eiumnoh, P. Praseartkul, et al., "Application of Infrared Thermography to Assess Cassava Physiology Under Water Deficit Condition," *Plant Production Science* 21, no. 4 (2018): 398–406, <https://doi.org/10.1080/1343943X.2018.1530943>.
18. F. Kalantari, O. M. Tahir, R. A. Joni, and E. Fatemi, "Opportunities and Challenges in Sustainability of Vertical Farming: A Review," *Journal of Landscape Ecology* 11, no. 1 (2018): 35–60, <https://doi.org/10.1515/jlecol-2017-0016>.
19. J. M. Roberts, T. J. A. Bruce, J. M. Monaghan, T. W. Pope, S. R. Leather, and A. M. Beacham, "Vertical Farming Systems Bring New Considerations for Pest and Disease Management," *Annals of Applied Biology* 176, no. 3 (2020): 226–232, <https://doi.org/10.1111/aab.12587>.
20. A. Singh, B. Ganapathysubramanian, A. K. Singh, and S. Sarkar, "Machine Learning for High-Throughput Stress Phenotyping in Plants," *Trends in Plant Science* 21, no. 2 (2016): 110–124, <https://doi.org/10.1016/j.tplants.2015.10.015>.
21. K. G. Liakos, P. Busato, D. Moshou, S. Pearson, and D. Bochtis, "Machine Learning in Agriculture: A Review," *Sensors* 18, no. 8 (2018): 2674, <https://doi.org/10.3390/s18082674>.
22. Z. Gao, Z. Luo, W. Zhang, Z. Lv, and Y. Xu, "Deep Learning Application in Plant Stress Imaging: A Review," *Agri* 2, no. 3 (2020): 430–446, <https://doi.org/10.3390/agriengineering2030029>.
23. A. V. Zubler and J. Y. Yoon, "Proximal Methods for Plant Stress Detection Using Optical Sensors and Machine Learning," *Biosens* 10, no. 12 (2020): 193, <https://doi.org/10.3390/BIOS10120193>.
24. S. Sankaran, J. M. Maja, S. Buchanon, and R. Ehsani, "Huanglongbing (Citrus Greening) Detection Using Visible, Near Infrared and Thermal Imaging Techniques," *Sensors* 13, no. 2 (2013): 2117–2130, <https://doi.org/10.3390/s130202117>.
25. S. E. A. Raza, H. K. Smith, G. J. J. Clarkson, et al., "Automatic Detection of Regions in Spinach Canopies Responding to Soil Moisture Deficit Using Combined Visible and Thermal Imagery," *PLoS One* 9, no. 6 (2014): e97612, <https://doi.org/10.1371/journal.pone.0097612>.
26. R. Calderón, J. A. Navas-Cortés, and P. J. Zarco-Tejada, "Early Detection and Quantification of Verticillium Wilt in Olive Using Hyperspectral and Thermal Imagery Over Large Areas," *Remote Sensing* 7, no. 5 (2015): 5584–5610, <https://doi.org/10.3390/rs70505584>.
27. F. Cao, F. Liu, H. Guo, W. Kong, C. Zhang, and Y. He, "Fast Detection of *Sclerotinia sclerotiorum* on Oilseed Rape Leaves Using Low-Altitude Remote Sensing Technology," *Sensors* 18, no. 12 (2018): 4464, <https://doi.org/10.3390/s18124464>.
28. C. Cortes and V. Vapnik, "Support-Vector Networks," *Machine Learning* 20, no. 3 (1995): 273–297, <https://doi.org/10.1007/BF00994018>.
29. V. A. Correa Galvis, P. J. Flood, and P. Kalaitzoglou, "Design and Management of Globally-Networked Plant Factories: Commercial Application and Future Opportunities," in *Advances in Plant Factories: New Technologies in Indoor Vertical Farming*, T. Kozai and E. Hayashi, eds. (Burleigh Dodds Science Publishing, 2023), 419–434, <https://doi.org/10.19103/AS.2023.0126.24>.
30. A. Prashar and H. G. Jones, "Assessing Drought Responses Using Thermal Infrared Imaging," in *Methods in Molecular Biology*, P. Duque, ed. (Humana Press, 2016), 209–219, [https://doi.org/10.1007/978-1-4939-3356-3\\_17](https://doi.org/10.1007/978-1-4939-3356-3_17).
31. F. Pedregosa, G. Varoquaux, A. Gramfort, et al., "Scikit-Learn: Machine Learning in Python," *Journal of Machine Learning Research* 12 (2011): 2825–2830.
32. P. Pawara, E. Okafor, L. Schomaker, and M. Wiering, "Data Augmentation for Plant Classification," in *Advanced Concepts for Intelligent Vision Systems. ACIVS 2017. Lecture Notes in Computer Science*, J. Blanc-Talon, R. Penne, W. Philips, D. Popescu, and P. Scheunders, eds., Vol. 10617 (Springer, 2017), 615–626, [https://doi.org/10.1007/978-3-319-70353-4\\_52](https://doi.org/10.1007/978-3-319-70353-4_52).
33. C. E. Reynolds-Henne, A. Langenegger, J. Mani, N. Schenk, A. Zumsteg, and U. Feller, "Interactions Between Temperature, Drought and Stomatal Opening in Legumes," *Environmental and Experimental Botany* 68, no. 1 (2010): 37–43, <https://doi.org/10.1016/j.envexpbot.2009.11.002>.
34. L. G. Teixeira Crusiol, M. R. Nanni, R. H. Furlanetto, et al., "UAV-Based Thermal Imaging in the Assessment of Water Status of Soybean Plants," *International Journal of Remote Sensing* 41, no. 9 (2020): 3243–3265, <https://doi.org/10.1080/01431161.2019.1673914>.
35. C. Pradawet, N. Khongdee, W. Pansak, W. Spreer, T. Hilger, and G. Cadisch, "Thermal Imaging for Assessment of Maize Water Stress and Yield Prediction under Drought Conditions," *Journal of Agronomy and Crop Science* 209, no. 1 (2023): 56–70, <https://doi.org/10.1111/jac.12582>.
36. E. Driesen, W. van den Ende, M. de Proft, and W. Saeys, "Influence of Environmental Factors Light, CO<sub>2</sub>, Temperature, and Relative Humidity on Stomatal Opening and Development: A Review," *Agron* 10, no. 12 (2020): 1975, <https://doi.org/10.3390/agronomy10121975>.

## Supporting Information

Additional supporting information can be found online in the Supporting Information section.